Applied Catalysis B: Environmental 117–118 (2012) 135–147

Contents lists available at SciVerse ScienceDirect

Applied Catalysis B: Environmental

journal homepage: www.elsevier.com/locate/apcatb

Structure evolution of nanocrystalline $Ce_{1-x}Pd_xO_{2-y}$ mixed oxide in oxidizing and reducing atmosphere: Reduction-induced activity in low-temperature CO oxidation

M. Kurnatowska, L. Kepinski*, W. Mista

Institute of Low Temperature and Structure Research, Polish Academy of Sciences, Okolna 2, 52-422 Wroclaw, Poland

ARTICLE INFO

Article history:
Received 18 October 2011
Received in revised form
17 December 2011
Accepted 22 December 2011
Available online 14 January 2012

Keywords:
Ce—Pd—O mixed oxide
Nanocrystalline Pd doped ceria
CO oxidation
Reducibility
TEM

ABSTRACT

Nanocrystalline (4–8 nm) $Ce_{1-x}Pd_xO_{2-y}$ mixed oxide ($0 < x < 0.3$), active in low temperature CO oxidation, has been prepared by microemulsion method. Thorough XRD, TEM, SEM-EDS, BET and FT Raman studies revealed that the oxide with $x < 0.2$ is a homogeneous solid solution structurally stable up to 800 °C in oxidizing atmosphere. In hydrogen, already at 500 °C segregation of Pd particles occurs, which exhibit preferential Pd (1 1 1)‖CeO_2 (1 1 1) orientation, preserved even after reduction at 800 °C. $Ce_{0.89}Pd_{0.11}O_{2-y}$ oxide showed reversible extraction–dissolution of Pd upon successive reduction–oxidation cycles at 500 °C, which is an example of "self-regenerative" property important for potential catalytic applications. Doping with Pd strongly hinders the sintering of ceria at high temperatures and enhances its reducibility at low temperatures (below 500 °C).

"As prepared", oxidized $Ce_{0.89}Pd_{0.11}O_{2-y}$ sample demonstrates moderate activity in CO oxidation (reaching 85% conversion at ~250 °C) similar to that of 3% Pd/CeO_2 prepared by impregnation. The activity improves dramatically (measurable CO conversion below room temperature and 100% conversion at ~120 °C) after pre-reduction at 400 °C in H_2. It appears that partially reduced Pd species, or extremely small particles (<1 nm) at the surface of ceria are responsible for the low temperature activity in CO oxidation. Such Pd species could be strongly bonded to the surface, e.g., exhibiting a special epitaxial orientation observed for larger Pd crystallites (~2 nm) formed during reduction at higher temperatures.

1. Introduction

Pd nanoparticles supported on ceria are very active catalysts of many important reactions. It has been shown that in some of them e.g., low temperature decomposition of methanol, low temperature oxidation of CO or coke gasification, ionic form of Pd is an active component [1–3]. This ionic form, described as Ce—Pd—O, is created as a result of strong interaction of Pd nanoparticles with an easily reducible ceria support and was identified in several works [3–5].

Traditional Pd/CeO_2 catalysts prepared by impregnation are prone to deactivation during catalytic process at elevated temperatures due to sintering of the metal phase which decreases a number of Ce—Pd—O sites. In oxidizing environment Pd particles can be easily oxidized to PdO crystallites, which show low activity e.g., in low temperature oxidation [6]. Various solutions were proposed to overcome these drawbacks and obtain more active and stable catalysts [4,5,7,8]. One way is preparation of $Ce_{1-x}Pd_xO_{2-y}$ solid solution, where Pd ions are uniformly, atomically dispersed in ceria matrix having —□—Pt^{2+}—O—Ce^{4+}— kinds of linkage [7,8] and the other is creation of a surface Ce—Pd—O species in impregnated Pd/CeO_2 catalyst by special, high temperature treatment [4,5]. $Ce_{0.89}Pd_{0.11}O_{2-y}$ mixed oxide with mean crystallite size of 8.6 nm was obtained by citric acid sol–gel method [7]. The oxide was active in CO oxidation (reaching 100% conversion at 200 °C) but severe deactivation occurred after successive H_2/O_2 treatment at 800 °C. It should be noticed that despite low nominal Pd content some PdO was observed in XRD pattern of the as prepared catalyst. $Ce_{1-x}Pd_xO_{2-y}$ mixed oxide containing maximum 3% Pd^{2+} in Ce sites was synthesized using a solution combustion method [8]. The sample with $Ce_{0.99}Pd_{0.01}O_{2-y}$ composition was shown to be very active in CO oxidation [8] and as a three way catalyst [9]. Disadvantages of oxides synthesized using solution combustion method are rather big crystallites (30–40 nm), wide crystallite size distribution, small amount Pd ions in the ceria lattice and their nonuniform distribution (enrichment at the surface) [8]. Very recently, Singh and Hegde [10] prepared single phase $Ce_{1-x}M_xO_{2-\delta}$ (M = Pt or Pd, $0 < x < 0.10$) nanocrystallites of 5 nm sizes using a sonication route. The oxides were quite stable and even after long term (10 h) annealing in air at

* Corresponding author at: Institute of Low Temperature and Structure Research, Polish Academy of Sciences, P.O. Box 1410, 50-950 Wroclaw, Poland.
Tel.: +48 71 343 50 21; fax: +48 71 344 10 29.
E-mail address: L.Kepinski@int.pan.wroc.pl (L. Kepinski).

0926-3373/$ – see front matter © 2012 Elsevier B.V. All rights reserved.
doi:10.1016/j.apcatb.2011.12.034

600 °C mean crystallite size increased only to ~8 nm, with no sign of any phase separation.

In the present work, we report the results of thorough studies on the microstructure and thermal stability of $Ce_{1-x}Pd_xO_{2-y}$ (x = 0–0.3) mixed oxide prepared using a microemulsion method. The oxide obtained has smaller crystallites and is more uniform chemically and morphologically than that obtained by combustion or sol–gel methods. Effect of redox pretreatment-induced structure changes in $Ce_{0.89}Pd_{0.11}O_{2-y}$ on its activity in low-temperature CO oxidation has been studied.

2. Experimental

Nanosized $Ce_{1-x}Pd_xO_{2-y}$ (x = 0–0.3) was synthesized by water in oil microemulsion method [11]. Triton X-100 was used as a non-ionic surfactant and cyclohexane and 1-pentanol as an organic phase. Water phase containing a solution of cerium and palladium nitrates was poured into organic phase and mixed for until transparent emulsion was obtained. Then the second reactant tetramethylammonium hydroxide (25% aqueous solution) was added and the microemulsion was mixed for 30 min. The organic phase was removed by decanting and the precipitated oxide was washed with acetone (two times) and then with methanol (four times). Finally the solid was separated by centrifugation, dried and then heated in oxygen at 500 °C for 2 h. 3 wt% Pd/CeO_2 was prepared by wet impregnation of nanosized CeO_2 with an aqueous solution of Pd nitrate, followed by heating in oxygen at 500 °C for 2 h.

The elemental ratios of Ce/Pd for all samples were confirmed by energy dispersive spectroscopy EDX (EDAX Pegasus XM4 spectrometer installed on FEI NovaNanoSEM 230). Morphology and microstructure were investigated by TEM (Philips CM20 Super-Twin at 200 kV). Analysis of HRTEM images was made with programs: Digital Micrograph (Gatan) and ImageJ [12]. XRD data were recorded by X'Pert Powder Diffractometer (PANanalytical) using CuKα radiation in the 2Θ range 10–110°. In situ XRD patterns were collected in static air in 2Θ range 25–62.5° for 50 min. Temperature accretion was 5°/min and sample was kept at each temperature for 10 min before data collecting. The phase composition, lattice parameter, size, micro strain and oxygen occupancy were determined with X'Pert HighScore Plus program using Rietveld refinement.

Surface area measurement S_{BET} was performed by the multipoint Brunauer–Emmet–Teller method (BET) with Sorptomatic 1900 FISONS instrument. Nitrogen sorption isotherms were obtained at liquid nitrogen temperature using a volumetric technique on samples out-gassed in a vacuum at 200 °C for 10 h. The total pore volume (V_p) was derived from the amount of nitrogen adsorbed at a relative pressure close to unity (P/P_o = 0.98) by assuming that all the accessible pores were then filled with liquid nitrogen. Pore size distribution and mean pore diameter (D_p) for mesopores was calculated from N_2-desorption isotherm by Barrett–Joyner–Halenda (BJH) method.

The Raman spectra were acquired with Bruker FT Raman spectrometer with resolution 2 cm^{-1} using Nd:YAG laser with emission line at 1064 nm. Temperature programmed reduction (H_2-TPR) was performed in a quartz microreactor by heating the sample up to 900 °C in H_2 (5 vol.%)/Ar flow (30 ml/min) with the heating rate of 10°/min. The hydrogen consumption was monitored by thermoconductivity (TCD) detector. Temperature programmed reduction (CO-TPR) was performed in the same quartz microreactor. Before each measurement, 50 mg sample was calcined in situ in 20% O_2/He (100 ml/min) at 500 °C for 1 h followed by cooling down to RT in He. A flow of 1% CO/He (100 ml/min) was then introduced as reducing agent and the sample was heated up to 900 °C at a rate of 10 °C/min. The signal of CO uptake as well as the H_2 production were acquired by an on-line Pfeiffer mass spectrometer (Omnistar QMS-200). Temperature-programmed oxidation (TPO) after the CO-TPR experiment was performed to study a re-oxidation process of the reduced surface and bulk of samples and also to detect any surface carbonaceous deposits formed during CO-TPR process. After finishing of CO-TPR experiment, the reactor was cooled down to room temperature, the reaction mixture was switched to a flow of 1% O_2/He, and temperature was increased to 900 °C at 10 °C/min. The CO_2 concentration was analyzed at the outlet of the reactor with a quadrupole mass spectrometer QMS-200 Omnistar.

A catalytic reaction test for CO oxidation was carried out in a flow microreactor at atmospheric pressure. The catalyst bed was heated from −40 °C to 300 °C at constant rate of 5 °C/min while supplying a gas mixture containing CO (1%), O_2 (1%), and He (balance) flowing at 100 ml/min. The effluent gas (CO, O_2 and CO_2) was analyzed by the on-line mass spectrometer (OmniStar QMS-200).

Thermal stability of the oxides in oxidizing and reducing conditions was checked by heating the samples in flow of oxygen at 800 °C, 850 °C and 900 °C for 2 h or in flow of hydrogen at 300 °C, 400 °C, 500 °C and 800 °C for 1 h.

3. Results and discussion

3.1. Structural characterization

Composition and homogeneity of the samples after heating in O_2 at 500 °C for 2 h (i.e., "as prepared" samples) was checked by EDS. The measured compositions (x = 0.015, 0.035, 0.052, 0.11, 0.16, 0.18, 0.21 and 0.31) were close to the nominal ones (0.01, 0.03, 0.05, 0.1, 0.15, 0.18, 0.20 and 0.30). Thorough, multi point EDS analysis for the sample with a nominal composition x = 0.1 gave a mean value x = 0.11 and point to point variations within ±0.02, indicating that no noticeable, macroscopic phase separation occurred during the sample preparation. Similar results were obtained for other samples.

The nitrogen adsorption/desorption isotherm and pore size distribution of the representative $Ce_{0.89}Pd_{0.11}O_{2-y}$ sample heated in oxygen at 500 °C are shown in Fig. S1 (supporting info). It can be concluded that the sample exhibits the classical shape of a type IV isotherm according to the IUPAC classification, typical for mesoporous solids. The pore size distribution (inset to Fig. S1) indicates a mesoporous structure and confirms a relatively narrow pore size distribution. The BET surface area, average pore diameter (D_p) and pore volume for the $Ce_{0.89}Pd_{0.11}O_{2-y}$ sample were 110 m^2/g, 3.8 nm and 0.105 cm^3/g, respectively. As expected the adsorption data revealed high dispersion of the oxide (BET surface area 110 m^2/g) and lack of microporosity. Average particle size evaluated from BET data using formula $d_{av} = 6000/(\rho \cdot S_{BET})$, where ρ = 6.96 [g/cm^3] – density of the oxide, is 7.8 nm, which is ~50% bigger than mean crystallite size of 5 nm obtained from XRD and TEM. The reason of this difference is agglomeration of the crystallites seen in TEM micrographs (Fig. 3).

XRD patterns for all "as prepared" $Ce_{1-x}Pd_xO_{2-y}$ (x = 0–0.3) samples are shown in Fig. S2 (supporting info). For x = 0–0.21, all reflections could be assigned to a fluorite structure of CeO_2 while for x = 0.31 very weak additional line corresponding to PdO was present. Several parameters: lattice parameter, mean crystallite size, micro strain, and oxygen occupancy were refined using X'Pert HighScore Plus program and are presented in Figs. 1 and 2. The refinement revealed linear growth of the lattice parameter of CeO_2 with Pd content up to x = 0.21 (Fig. 1). The value of the lattice parameter for x = 0.31 was close to that for x = 0.21 indicating that maximum Pd incorporation was exceeded and some Pd did not enter the ceria lattice but formed highly dispersed PdO at the surface. The observed lattice expansion with increasing Pd content

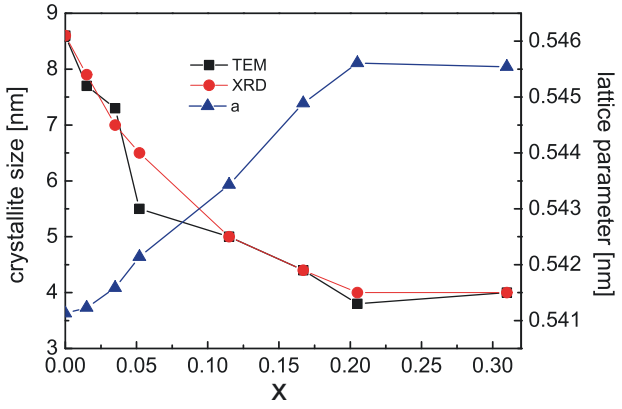

Fig. 1. Mean crystallite sizes and lattice parameters measured for $Ce_{1-x}Pd_xO_{2-y}$ samples.

seems to contradict the results of Priolkar et al. [8], who reported the opposite trend for $Ce_{0.89}Pd_{0.11}O_{2-y}$ obtained by the combustion method. The effect was explained by the fact that the radius of Pd^{2+} 86 pm, is smaller than that of Ce^{4+} −87 pm (for the same coordination VI) [13]. It should be noted however, that the difference in the radii is very small and in our opinion the disparate behavior is rather due to difference in the mean crystallite size of the mixed oxide: 30–40 nm in [8] and 4–8 nm in this work. For $Ce_{1-x}Pd_xO_{2-y}$ samples prepared using sonication method and having mean crystallite size ~5 nm, i.e., similar to our, an increase of the lattice parameter of CeO_2 with Pd content was observed [10].

From Fig. 1 it appears that the mean crystallite size of the mixed oxide decreases with increasing Pd content, so that for $x = 0.21$ it is 4 nm, i.e., two times smaller than for bare CeO_2. It causes a problem with interpretation of the observed change of the lattice parameter with Pd doping due to well known dependence of the lattice parameter of CeO_2 on the mean crystallite size [14–16]. The expansion of CeO_2 lattice with decreasing crystallite size is explained by various factors such as modification of surface energy by adsorbed species [14] or presence of Ce^{3+} ions and oxygen vacancies in the lattice [15,16]. All these effects may also occur for the $Ce_{1-x}Pd_xO_{2-y}$ with additional one i.e., replacement of Ce^{4+} ions with Pd^{2+} ions having different charge and slightly smaller ion radius. In our opinion the decline of the mean crystallite size of ceria with increasing Pd content (cf. Fig. 1) and generation of additional oxygen vacancies is mainly responsible for the observed growth of the lattice parameter. The results of the Rietveld refinement confirmed an expected decline of the oxygen occupancy with Pd loading and revealed also the presence of micro strain (Fig. 2).

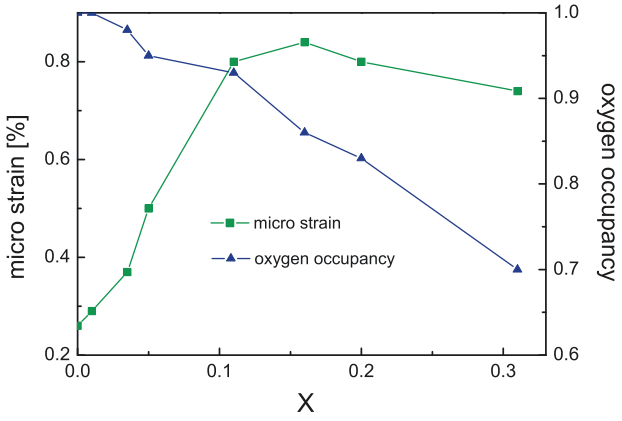

Fig. 2. Micro strain and oxygen occupancy refined for $Ce_{1-x}Pd_xO_{2-y}$ using Rietveld method.

An unexpected result is further decline in oxygen occupancy and microstrain for $x = 0.31$, i.e. above estimated maximum solubility of Pd ($x = \sim 0.21$). This apparent inconsistency arose, probably, due to errors in the structure refinement procedure, where we did not take into account a small amount of PdO occurring for $x = 0.31$ (cf. Fig. S2 in supporting info). Due to overlapping of some $Ce_{1-x}Pd_xO_2$ and PdO reflections accuracy of refinement of the structure parameters influencing intensity and shape of the reflections is poorer than for pure oxide. It applies in particular to oxygen occupancy and microstrain presented in Fig. 2.

Examples of HRTEM images of $Ce_{1-x}Pd_xO_{2-y}$ heated in O_2 at 500 °C for 2 h are shown in Fig. 3 for $x = 0.11$ and 0.16. Analysis of the images revealed that the samples contained well defined nanocrystals with a narrow size distribution. The crystallites do not exhibit any special crystal form and thus various crystal planes are exposed. Mean crystallite size was calculated for all samples from several HRTEM images and the results are presented in Fig. 1 and compared with mean crystallite sizes calculated from XRD. As it is seen there is a good agreement between both sets of data.

3.2. Raman spectroscopy

Fig. 4a shows Raman spectra of "as prepared" $Ce_{1-x}Pd_xO_{2-y}$ samples for $x < 0.2$. Measurement of Raman scattering for higher doping was not possible because of heating caused strong radiation absorption. The spectra are dominated by a strong band near 464 cm^{-1}, which is assigned to vibration mode of F_{2g} symmetry in the cubic lattice of CeO_2 [15–17]. With increasing Pd content the band weakens, shifts to lower frequency and broadens asymmetrically (inset to Fig. 4a). In accordance with XRD data presented above, all these effects can be attributed to morphological changes, i.e., decreasing mean crystallite size, increasing lattice parameter and increasing disorder (strain). Such effects are very well documented in literature for nanocrystalline bare and doped CeO_2 [16–18] and can be considered as an evidence of Pd incorporation into ceria lattice.

For the samples with $x \geq 0.05$, additional bands occurred at 185 cm^{-1} and 500–650 cm^{-1}. Such bands, frequently reported in literature are usually assigned to the presence of defects in the ceria lattice [19]. Nakajima et al. [20] reported the presence of similar bands in Raman spectra of doped coarse crystalline CeO_2. For Y and La doped CeO_2 the bands occurred at ~250, ~540 and ~600 cm^{-1}, while for Zr doped CeO_2 only band at ~600 cm^{-1} was observed. The later band was assigned to defects containing dopant ion occupying Ce^{4+} site in MO_8 coordination. The other bands at ~250 and ~540 cm^{-1} were assigned to defects that include oxygen vacancies, generated to maintain electroneutrality, with symmetry different from that of O_h point group. Defect induced low frequency bands were observed also in Raman spectra of nanocrystalline CeO_2 doped with Lu at 252 cm^{-1} [21] but also with Y at 257 cm^{-1} (Fig. 4b). No such band was observed for nanoceria doped with Zr (Fig. 4b). $Ce_{0.9}Zr_{0.1}O_2$, $Ce_{0.9}Lu_{0.1}O_{2-y}$ and $Ce_{0.9}Y_{0.1}O_{2-y}$ oxides were prepared according to the procedure described in [21]. For $Ce_{1-x}Pd_xO_{2-y}$ studied in this work the bands at ~540 and ~600 cm^{-1} merged into one broad band, but the low energy band is strongly shifted toward lower frequency (185 cm^{-1}). It should be noticed that the band at 185 cm^{-1} cannot be assigned to PdO, which shows Raman bands at 651 cm^{-1} (strong) and at 278, 445, 725 cm^{-1} (weak) [22]. Recently, similar low frequency band was observed in Raman spectra of $Ce_{1-x}Ni_xO_{2-y}$ ($x = 0.1$ and 0.12) at around 230 cm^{-1} [23] and at 175 cm^{-1} for $Ce_{1-x}Cu_xO_{2-y}$ ($x = 0.1$ and 0.2) [24]. Calculations of density of state of CeO_2 show that the spectrum can be divided into a part originating from the cerium and the oxygen [25]. Because of the large mass difference between cerium and oxygen the low frequency vibrations are dominated by the motion of heavy cerium ions. Replacement of Ce^{4+} ions with

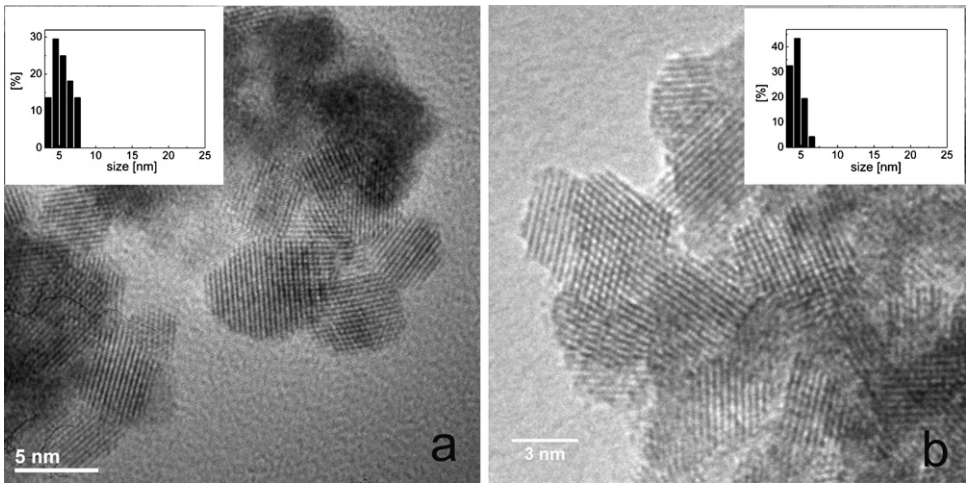

Fig. 3. HRTEM images of $Ce_{1-x}Pd_xO_{2-y}$ heated in O_2 at 500 °C for 2 h (a) for $x = 0.11$ and (b) 0.16. Insets present crystallite size distributions.

other element should therefore effect a low frequency part of the Raman spectrum. In the case of aliovalent dopants there is additional distortion of the local symmetry because of the presence of oxygen vacancies, which are situated close to the dopant ions. Recent calculations suggest that for Pd doped CeO_2 the symmetry distortion could be exceptionally large due to a tendency of Pd^{2+} ions to assume square PdO_4 coordination, quite different from cubic CeO_8 coordination [26]. This could explain relatively high intensity and large shift of the low frequency band for $Ce_{1-x}Pd_xO_{2-y}$. It should be mentioned however, that some authors assign the occurrence of the additional low frequency bands in CeO_2 doped with Cu [24] or Ca [27] to small tetragonal distortion of a cubic lattice of ceria.

3.3. Thermal stability $Ce_{0.89}Pd_{0.11}O_{2-y}$ in oxygen and in hydrogen

Detail study of the thermal stability of the $Ce_{1-x}Pd_xO_{2-y}$ upon heat treatment in oxidizing and reducing atmosphere was studied for one selected composition $x = 0.11$, which according to above data showed no evidence of phase separation after preliminary treatment at 500 °C.

3.3.1. Oxygen

Fig. S3 (supporting info) depicts XRD patterns of $Ce_{0.89}Pd_{0.11}O_{2-y}$ sample heated in oxygen at 800 °C, 850 °C and 900 °C for 2 h. All the patterns contain intense reflections of the fluorite structure, but for the samples heated at 850 °C and 900 °C there is a small, additional feature close to (2 0 0) fluorite reflection at ~34° which may origin from the strongest PdO (0 1 1) reflection. Results of Rietveld refinement for the patterns shown in Fig. S3 are summarized in Table 1. It appears that there was some sintering of $Ce_{0.89}Pd_{0.11}O_{2-y}$ at 800 °C, but obviously addition of Pd strongly inhibited growth of ceria crystallites. The effect is also clearly seen in Fig. S4 showing TEM images and crystallite size distributions of $Ce_{0.89}Pd_{0.11}O_{2-y}$ and CeO_2 samples heated at 800 °C. The inhibiting effect of doping with various elements on sintering of CeO_2 is well documented in literature [28]. More severe sintering of $Ce_{0.89}Pd_{0.11}O_{2-y}$ occurred at 850 °C and especially at 900 °C. The effect correlates with decrease of the lattice parameter and precipitation of PdO: 3.6 wt% and 6.2 wt%, respectively. Since Pd content in the "as prepared"oxide corresponded to 8 wt% PdO, then small amount of Pd still remained in the ceria lattice after heating at 900 °C. For $Ce_{1-x}Pd_xO_{2-y}$ samples with $x \geq 0.16$ segregation of PdO was observed already after heating at 800 °C.

The microstructure of the $Ce_{0.89}Pd_{0.11}O_{2-y}$ subjected to high temperature treatment was studied by HRTEM. No crystalline PdO could be identified in HRTEM images of the sample heated at 850 °C, but very thin amorphous layer was visible at the surface of ceria crystallites (Fig. 5a). The amorphous layer mostly vanished after heating at 900 °C and small PdO crystallites (4–6 nm) appeared at the surface of ceria instead (Fig. 5b). Interestingly, in addition to large crystallites of ceria with size of few tens of nm, HRTEM images of the sample heated at 900 °C revealed the presence of very small ones with size 2–3 nm (Fig. 5c). The origin of such

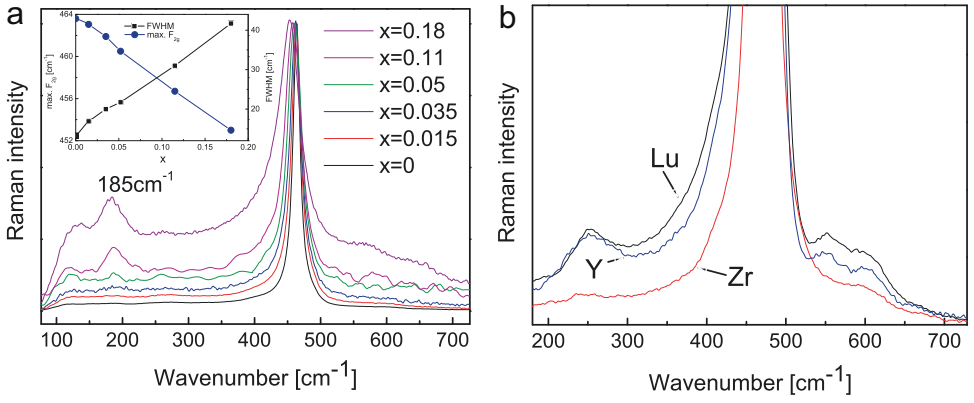

Fig. 4. (a) Raman spectra of $Ce_{1-x}Pd_xO_{2-y}$ ($x = 0$–0.18). Inset presents Raman shift (circles) and half width (squares) of the F_{2g} mode. (b) Raman spectra of $Ce_{0.9}Zr_{0.1}O_2$ (red), $Ce_{0.9}Lu_{0.1}O_{2-y}$ (black) and $Ce_{0.9}Y_{0.1}O_{2-y}$ (blue). (For interpretation of the references to color in this figure legend, the reader is referred to the web version of the article.)

Table 1
XRD and TEM results for CeO_2 and $Ce_{0.89}Pd_{0.11}O_{2-y}$ subjected to heating in oxygen.

Sample	Mean size [nm]		Lattice parameter [nm]	Phase separation
	XRD	TEM		
CeO_2 as prepared	8.6	8.5	0.541(1)[a]	–
CeO_2 800 °C	56.4	56	0.541(0)	–
$Ce_{0.89}Pd_{0.11}O_{2-y}$ as prepared	5	5	0.543(6)	–
$Ce_{0.89}Pd_{0.11}O_{2-y}$ 800 °C	14	13.5	0.542(1)	–
$Ce_{0.89}Pd_{0.11}O_{2-y}$ 850 °C	20	24(3–40)	0.541(7)	PdO 3.6 wt%
$Ce_{0.89}Pd_{0.11}O_{2-y}$ 900 °C	36	32(3–50)	0.541(4)	PdO 6.2 wt%

[a] The estimated standard deviations are <0.0001 nm.

particles is unclear, but it may be connected with the process of phase separation. During cooling in oxygen, the smallest Pd particles, formed at the surface at 900 °C, may react with the surface of Pd depleted mixed oxide to restore the initial composition. Possibility of such process is validated by the results of successive reduction–oxidation treatments described below.

3.3.2. *In situ XRD*

In situ XRD was performed during heating of $Ce_{0.89}Pd_{0.11}O_{2-y}$ sample in static air from room temperature to 850 °C (Fig. 6a) and then cooling back to RT (Fig. 6b). On heating very weak reflection from PdO (0 1 1) became visible at ~34° at 780 °C and grew in intensity up to 825 °C. Simultaneously weak Pd (1 1 1) reflection appeared at around 825 °C at ~40°. At 850 °C intensity of Pd (1 1 1) increased significantly though weak PdO reflection was still present. It is interesting observation because temperature of PdO decomposition to Pd in air is 800 °C for bare PdO [29] and 810 °C for PdO/Al_2O_3 catalyst [30]. The effect is probably caused by a strong interaction of PdO with surface of ceria which, as it was suggested by Hinokuma et al. [5], is responsible for an increase of the temperature of dissociation of PdO on CeO_2 to 900 °C. Fig. 6b shows XRD patterns recorded on cooling of the samples in air. Down to 740 °C Pd was the only phase, but at 720 °C PdO became the prevailing phase. It appears therefore that Pd—PdO transformation is rather sharp and occurs at temperature 100 °C lower than PdO—Pd transformation during heating (Fig. 6a). This difference is caused by the fact that different processes operate in both cases. Formation of Pd crystallites during heating cycle requires a breakage of Pd—O—Ce bonds and diffusion of Pd from bulk to the surface of ceria lattice. Transformation of Pd crystallites (with mean crystallite size of a few nm) into PdO during cooling is just an oxidation process. Dynamical changes of the Pd and PdO content in the $Ce_{0.89}Pd_{0.11}O_{2-y}$ sample during heating and cooling are shown in Fig. 7b. An unexpected observation is that maximum of Pd content is achieved at 800 °C during cooling cycle and not during heating at 850 °C. The reason is a slow kinetics of the PdO decomposition process. As can be seen in Fig. 6b the XRD pattern of the sample at 850 °C contains weak reflections of PdO, which disappeared after cooling to 800 °C (Fig. 6b) and increased the intensity of Pd reflections. The maximum Pd content equal to 5 wt% corresponds well with 5.3 wt% PdO content at room temperature after cooling. Similar effect of Pd—PdO hysteresis upon heating–cooling was first observed for PdO/alumina catalyst [30]. The width of the hysteresis can by decreased by suitable additives (e.g., ceria), which increases the temperature of Pd reoxidation during cooling [30]. Relatively high temperature of Pd reoxidation observed in this work (720 °C, Fig. 7a) agrees well with that reported Pd/CeO_2 [30] and $Pd/CeO_2/Al_2O_3$ catalyst [31] for similar O_2 partial pressure (21%). This temperature is ~150 °C higher than that for Pd/Al_2O_3 [30,31] and proves the beneficial role of $Ce_{1-x}Pd_xO_{2-y}$ in reoxidation of Pd and thus its applicability as high temperature combustion catalyst. Fig. 7a presents temperature dependence of lattice parameter and particle size of ceria. A linear increase of the lattice parameter with temperature on heating up to ~750 °C is the result of thermal expansion. At higher temperatures lattice parameter decreases because of irreversible processes of increase of the mean crystallite size and segregation of Pd from the ceria lattice. It is seen that crystallite growth of ceria begins around 600 °C but becomes rapid above 750 °C. Clearly, this effect is correlated with a decrease of the lattice parameter of ceria and appearance of PdO (cf. Fig. 7a). There are some differences in the results of in situ and ex situ XRD studies that should be explained. In particular the amount of PdO phase observed in the sample heated at 850 °C in oxygen for 2 h and cooled to RT (3.6 wt%) is much less than the amount observed after in situ experiment with heating to the same temperature in air (5.3 wt%). Moreover, mean crystallite size of PdO is significantly higher in the later case. Despite different sample history (various treatment procedure) the most important factor is gas atmosphere. It has been shown, that decomposition temperature of PdO depends on oxygen partial pressure in the O_2—N_2 gas mixture [29]. For 0.2 O_2 fraction (air composition) it is ~50 °C lower than in pure oxygen (850 °C).

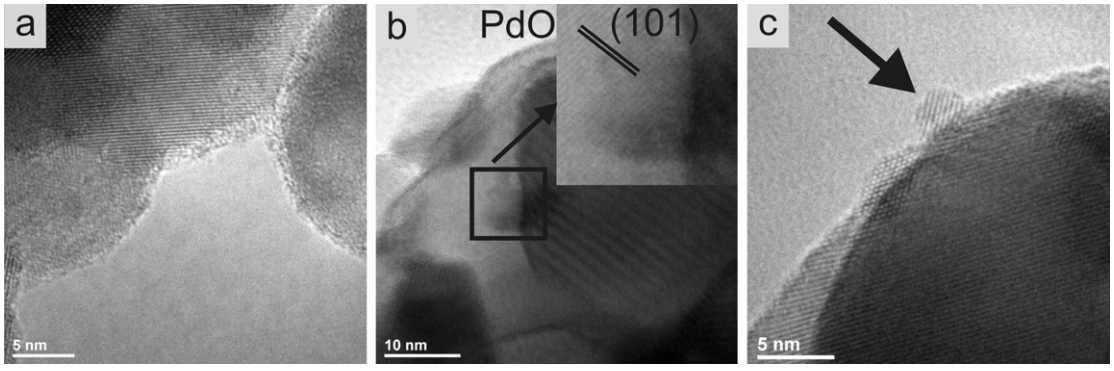

Fig. 5. TEM images of $Ce_{0.89}Pd_{0.11}O_{2-y}$ after heating in oxygen (a) at 850 °C and (b, c) at 900 °C.

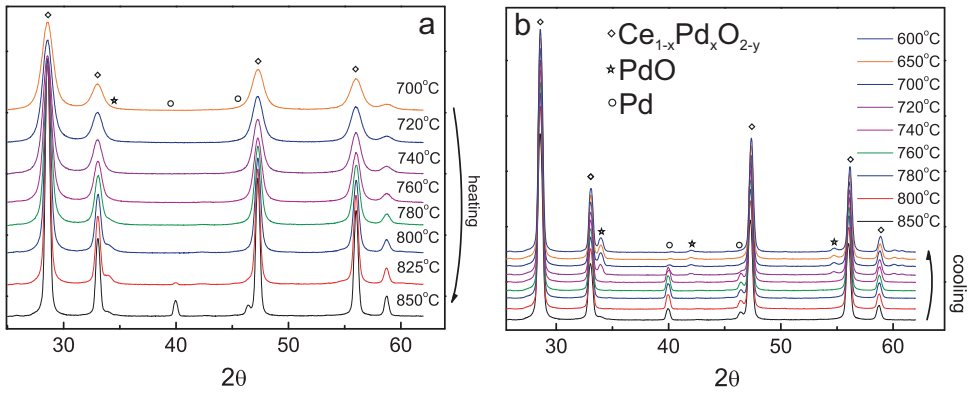

Fig. 6. "In situ" XRD patterns of $Ce_{0.89}Pd_{0.11}O_{2-y}$ recorded during (a) heating and (b) cooling in air. Peaks assignment: (diamonds) $Ce_{1-x}Pd_xO_{2-y}$, (stars) PdO and (circles) Pd.

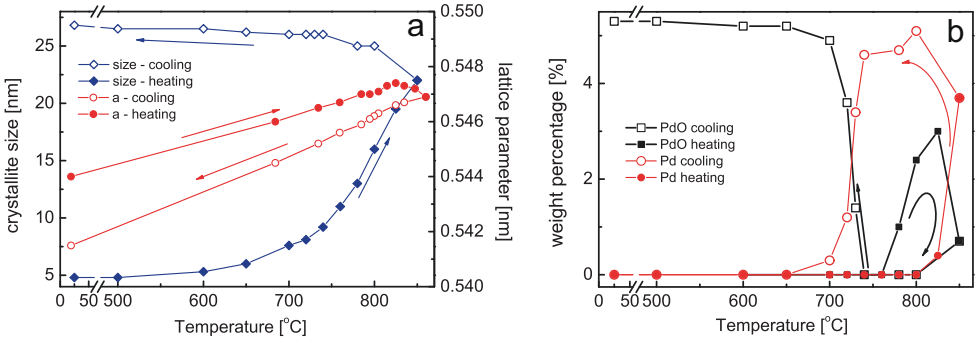

Fig. 7. Temperature dependence of lattice parameter and mean crystallite size (a) and content of Pd and PdO phases (b) for $Ce_{0.89}Pd_{0.11}O_{2-y}$ obtained from "in situ" XRD (full symbol – heating, open symbol – cooling).

3.3.3. Hydrogen

Fig. 8 presents XRD patterns of the $Ce_{0.89}Pd_{0.11}O_{2-y}$ sample heated in hydrogen for 1 h at 300 °C, 400 °C, 500 °C and 800 °C. After heating at 300 °C and 400 °C decrease in the lattice parameter and some growth of the mean crystallite size was noticed (see Table 2), with no evidence of phase separation. There is a question on the reason of the observed decrease of the lattice parameter. It appears that factors considered before i.e., change of the crystallite size or Pd segregation must be excluded. Other possible factor – reduction of Ce^{4+} with simultaneous generation of oxygen vacancies is known to increase the lattice parameter of ceria nanoparticles [15,16]. There must be therefore something else. Xu et al. [14] reported that expansion of the lattice parameter of very small CeO_2 particles (<5 nm) is caused by increasing surface energy due to creation of superoxides at the surface. Heating in reducing atmosphere would remove the peroxides decreasing thus the surface energy and then also the lattice parameter. After heating at 500 °C the mean size of ceria crystallites increased to 12 nm with further reduction of the lattice parameter. Moreover, weak and very broad diffraction peak from Pd (1 1 1) appeared at around 40° (Fig. 8). At 800 °C mean size of ceria and palladium crystallites reached 50 nm and 14 nm, respectively, and the amount of Pd was evaluated as 6 wt% (see Table 2). The lattice parameter of ceria decreased to the value close to that of pure CeO_2.

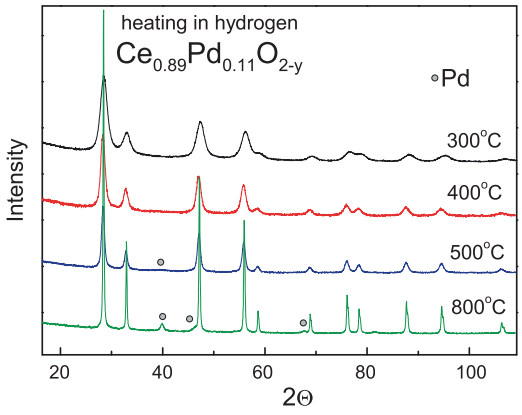

Fig. 8. XRD patterns of $Ce_{0.89}Pd_{0.11}O_{2-y}$ heated in hydrogen at 300 °C (black), 400 °C (red), 500 °C (blue) and 800 °C (green). (For interpretation of the references to color in this figure legend, the reader is referred to the web version of the article.)

HRTEM observations showed no clear evidence of any Pd particles in the sample reduced at 300 °C and 400 °C and the presence of small Pd particles (about 2 nm) in the sample heated at 500 °C (Fig. 9). Identification of such small Pd particles on ceria in HRTEM images was possible thanks to the presence of Moire fringes that form as the result of superposition of Pd and ceria crystal lattices. Wide ~0.8 nm Moire fringes seen in Fig. 9 are the result of interference of electron beams diffracted by parallel Pd (1 1 1) and ceria (1 1 1) lattice planes. Most of the observed Pd particles show such Moire fringes indicating, that Pd crystallites grow at the surface of the mixed oxide assuming a special epitaxial orientation such that (1 1 1) lattice planes of the metal and the oxide are parallel. The same effect was observed for Pd particles, as well as other metals deposited on CeO_2 by impregnation [3,30]. It was proposed that epitaxially oriented palladium clusters are quasi two dimensional and in this form can be more stable and resistant to oxidation to PdO [3]. There is also some shift of electron density from palladium to the support, resulting in charging Pd particles. Such flat Pd–ceria structures may be very active, appearing to be most suitable for optimal CO activation [3]. After heating at 800 °C larger Pd particles occurred in the sample, but there is still a fraction of small ones (~2 nm) (Fig. 9b). It appears that despite high temperature of reduction and significant increase of the size of Pd particles up

Table 2
XRD and TEM results for $Ce_{0.89}Pd_{0.11}O_{2-y}$ sample subjected to heating in hydrogen.

Sample treatment:	XRD Rietveld refinement			TEM	
	Mean size [nm]	*a* [nm]	Phase separation	Mean size [nm]	Phase separation
As-prepared	5	0.5436	–	5	–
300 °C/1 h H_2	5.7	0.5425	–	5	–
400 °C/1 h H_2	8.7	0.5418	–	8.3	–
500 °C/1 h H_2	12	0.5416	Pd, v. weak	12	Pd ~2 nm
800 °C/1 h H_2	50	0.5412	Pd, 14 nm, 6 wt%	50 (20–70)	Pd 2–10 nm

to ~8 nm the epitaxial Pd (1 1 1)‖CeO_2 (1 1 1) orientation was preserved. The largest particles (10–13 nm) did not show however any special orientation relative to the support.

It is interesting to compare a structure of the $Ce_{0.89}Pd_{0.11}O_{2-y}$ sample subjected to heat treatment in oxygen and in hydrogen. Most striking fact is much faster sintering of ceria in hydrogen. Heating at 800 °C increased the mean crystallite size from 5 nm to 14 nm or to 50 nm, in O_2 and H_2, respectively. The reason could be extraction of Pd from the ceria lattice in hydrogen atmosphere what destroys an inhibiting effect of Pd on the crystallite growth of ceria. From Table 1 it appears that mean crystallite size of bare CeO_2 heated in O_2 at 800 °C (56 nm) is close to that of $Ce_{0.89}Pd_{0.11}O_{2-y}$ heated in H_2 at the same temperature. There is also strong effect of the atmosphere on the stability of the mixed oxide. In oxidizing atmosphere no PdO phase could be detected after heating at 800 °C, while well developed 2 nm Pd particles occurred already after heating at 500 °C in hydrogen. The reason is very high stability of Pd—O—Ce bonds existing at the surface of CeO_2 in oxidizing environment [4,5] thanks to special square-planar $Pd^{2+}O_4$ coordination similar to that in PdO [4]. Recent calculations showed that similar quasi planar $Pd^{2+}O_4$ coordination should be preferred also for Pd^{2+} ions substituted for Ce^{4+} in diluted $Ce_{1-x}Pd_xO_{2-y}$ solid solutions [26].

Wang et al. [7] studied the effect of H_2 and O_2 treatment at 800 °C on the structure and activity of Pd doped CeO_2 (1:99 Pd:Ce molar ratio) prepared by sol–gel method. The initial sample contained ceria crystallites with mean size of 8.6 nm, which after treatment in air at 800 °C for 5 h increased to 42 nm. Similar as in our case heating of the initial sample in hydrogen at the same temperature caused much more severe sintering of ceria (mean crystallite size of 69 nm) and moreover segregation of Pd as a separate phase.

HRTEM revealed that in $Ce_{0.89}Pd_{0.11}O_{2-y}$ sample reduced in hydrogen at 500 and 800 °C wide 0.58 or 0.9 nm fringes occurred sometimes on ceria crystallites in addition to 0.31 nm fringes from (1 1 1) lattice planes (Fig. 10). There are two possible origins of the additional fringes. The first is superstructure formed as the result of generation and ordering of oxygen vacancies often observed for pure or doped ceria [32–34]. An alternate explanation is Pd—Ce—O surface superstructure observed in Pd/CeO_2 catalysts subjected to high temperature treatment in air at 900 °C [4]. We would rather prefer the first possibility because of the reducing atmosphere used in our case and the appearance of the HRTEM images. It appears that intensity of the superstructure fringes observed in plane view on a crystallite with a thickness of 5 nm or more is too strong to be explained by a monolayer surface reconstruction. In order to reveal such surface reconstruction in TEM profile imaging is required. Interestingly and unexpectedly, such reconstruction is not visible in the profile view HRTEM image in [4].

3.3.4. *Successive reduction and oxidation*

Effect of successive reduction and oxidation at 500 °C on the structure of $Ce_{0.89}Pd_{0.11}O_{2-y}$ sample is shown in Fig. 11. It is seen, that very weak Pd (1 1 1) reflection which occurred due to reduction at 500 °C disappeared during subsequent oxidation treatment, and no PdO reflections showed up instead. At the same time, small increase of the mean crystallite size and the lattice parameter of the mixed oxide was observed (Table 3). Accordingly, HRTEM revealed the disappearance of Pd particles with characteristic parallel Moire fringes and occurrence of small particles with fringes characteristic for the mixed oxide (Fig. 12). No PdO particles could be found in the images but morphology of $Ce_{0.89}Pd_{0.11}O_{2-y}$ crystallites became more irregular. In particular, edges of the crystallites are rough and contain patches of very thin amorphous phase. These observations supported by XRD data (increase of the lattice parameter of ceria and increase of micro strain) indicate that Pd formed upon reduction diffused back into ceria lattice during oxidation treatment at 500 °C. In order to check reversibility of the process the reduction and re-oxidation cycle was performed three times. As it appears from Fig. 11 and Table 3 the cycling caused just appearance and disappearance of small Pd reflections in XRD diffractograms with no noticeable change of the structural parameters of the mixed oxide. In addition, diffractogram of the sample subjected to second

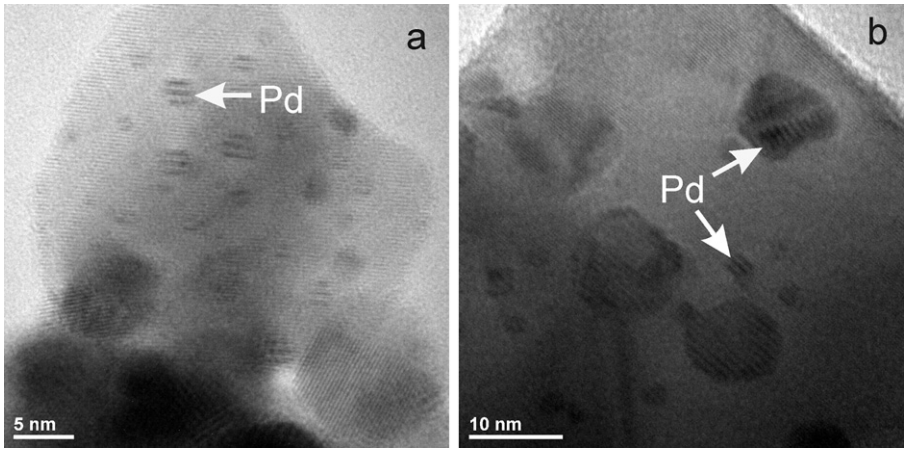

Fig. 9. HRTEM images of $Ce_{0.89}Pd_{0.11}O_{2-y}$ heated in hydrogen at 500 °C and 800 °C.

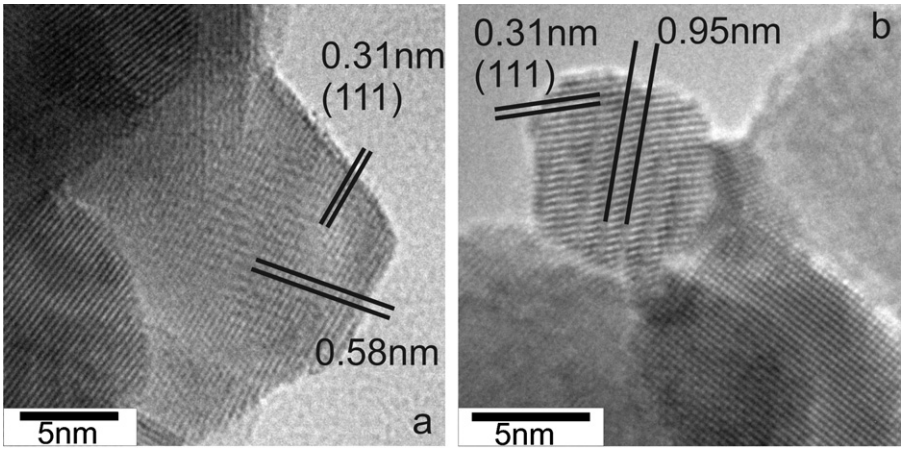

Fig. 10. Superstructure fringes in HRTEM images of $Ce_{0.89}Pd_{0.11}O_{2-y}$ heated in hydrogen at 800 °C (a) and at 500 °C (b).

Table 3
XRD and TEM results for $Ce_{0.89}Pd_{0.11}O_{2-y}$ sample subjected to alternate heating in hydrogen and oxygen.

Sample treatment:	XRD Rietveld refinement			XRD pattern	TEM
	Mean size [nm]	*a* [nm]	Micro strain [%]	Phase separation	Phase separation
As-prepared	5	0.5436	0.81	–	
Reduction 500 °C	12	0.5416	0.05	Pd, v. weak	Pd, ~2 nm
Re-oxidation 500 °C	14	0.5420	0.19	–	
Reduction 500 °C	16	0.5413	0.05	Pd, v. weak	Pd, ~2 nm
Re-oxidation 500 °C	16	0.5417	0.19	–	
Reduction 500 °C	16	0.5413	0.05	Pd, v. weak	Pd, ~2 nm

reoxidation contains a very weak, broad feature at ~34 that could be due to traces of PdO. It raises a possibility that the process of extraction–dissolution is not fully reversible.

Similar behavior was reported for $Ce_{1-x}Cu_xO_{2-y}$ solid solution [24], where extraction–dissolution of Cu was observed following change of gas atmosphere from reducing to oxidizing during in situ XRD measurement at 300 °C. As in our case, no crystalline copper oxide phase was observed. Recent, "in situ" XRD, HRTEM and XANES studies on reduction–oxidation cycling of nanocrystalline $Ce_{0.8}Cu_{0.2}O_{2-y}$ revealed that the extraction–dissolution of Cu is only partly reversible [35]. About half of Cu present in the ceria lattice in the initial sample remained at the surface as an amorphous CuO_x phase after reduction–oxidation treatment at 400 °C [35]. According to HRTEM thickness of this phase may reach up to 10 nm [35]. In our case no evidence of such large amount of amorphous phase was detected in HRTEM micrographs, though patches of very thin (~1 nm) amorphous layer were observed (Fig. 12b). Results of XRD measurements (Table 3) show some irreversible decrease of the lattice parameter after first reduction–oxidation cycle at 500 °C, but we assign it rather to significant growth of the mean size of the ceria crystallites. In further cycles the changes are small and reversible. The concept of extraction–dissolution of metal phase in complex oxides is a basis of so called "self-regenerative property" discovered for Pd-doped perovskite catalyst for automotive emission control [36]. Recently, similar reversible process of formation of 1–2 nm metallic Pt particles in reducing atmosphere and their spreading into oxidized monolayer in oxidizing atmosphere was found in Pt/CeO_2 catalyst [37]. The authors explain the formation of this stable surface Pt—O oxide by the strong interaction between oxidized Pt and CeO_2 that involves the formation of a Pt—O—Ce bond.

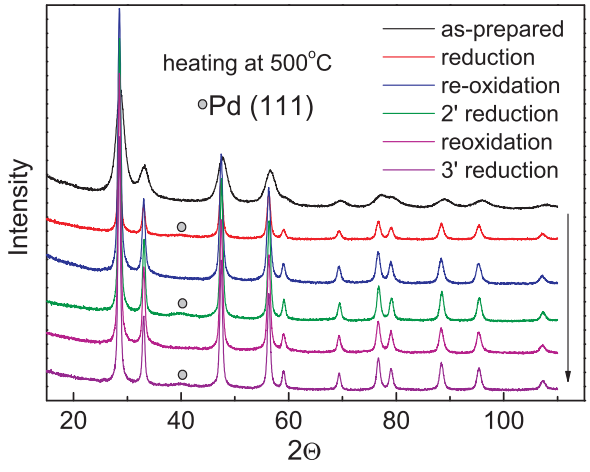

Fig. 11. XRD patterns of $Ce_{0.89}Pd_{0.11}O_{2-y}$ heated alternately in H_2 and O_2 at 500 °C.

3.4. Reducibility

3.4.1. H_2-TPR

The reduction properties of the catalysts were analyzed by H_2-TPR up to 920 °C. Fig. 13 shows TPR profiles for $Ce_{0.89}Pd_{0.11}O_{2-y}$ sample (two successive runs – Fig. 13a) and 3 wt% Pd/CeO_2 prepared by impregnation (Fig. 13b). On the profiles three regions of hydrogen consumption can be distinguished. Low temperature region below 250 °C which is related to reduction of Pd species, middle temperature region 250–500 °C related to reduction of surface Ce^{4+} ions, and high temperature region above 500 °C related to bulk reduction of ceria.

3.4.2. I H_2-TPR run for $Ce_{0.89}Pd_{0.11}O_{2-y}$

The H_2-TPR profile (Fig. 13a) shows four broad reduction peaks at ca. 150, 335, 460 and 787 °C. Precise peak shape analysis revealed however, that the peak centered at 150 °C can be deconvoluted into three components: main peak at 150 °C (67%) and two shoulders

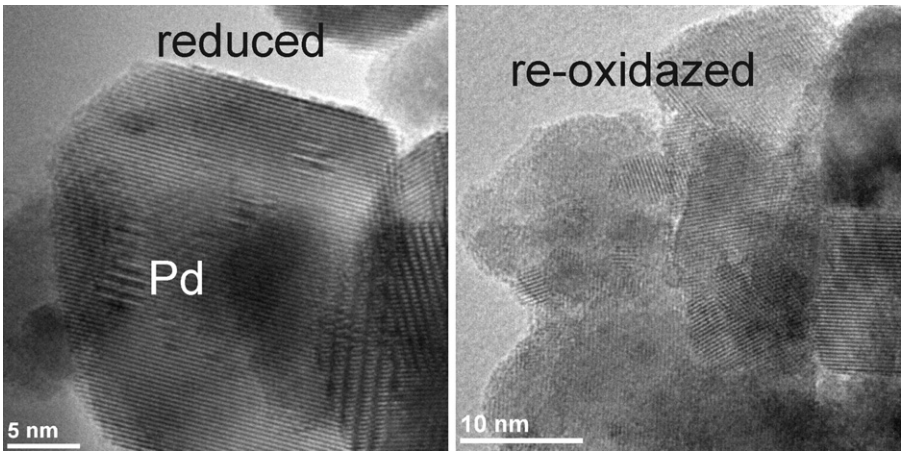

Fig. 12. HRTEM images of $Ce_{0.89}Pd_{0.11}O_{2-y}$ heated alternately in H_2 and O_2 at 500 °C.

at 105 °C (13%) and 200 °C (20%). The first small peak at 105 °C could be assigned to the reduction of traces of PdO phase present at the surface of the sample [52], while the main peak at 150 °C and the shoulder at 200 °C can be assigned to the reduction of ionic Pd^{2+}-like species at the surface and sub-surface region of the solid solution forming —Pt^{2+}—O—Ce^{4+}— linkage. We admit, however, in agreement with [52], that this reduction peak may contain simultaneous reduction of some Ce^{4+} ions in close vicinity of Pd clusters. The low temperature part of TPR profile of $Ce_{0.89}Pd_{0.11}O_{2-y}$ differs clearly from that of 3 wt% Pd/CeO_2 calcined in air at 500 °C (Fig. 13b), which contains single, strong peak at ~70 °C due to reduction of PdO. The peak is distorted because of superposition with a negative peak due to decomposition of Pd hydride formed during H_2-TPR [38,39]. It has been established that redox behavior for Pd/CeO_2 catalysts, especially position of the low temperature peaks strongly depends on the preparation method and Pd content. Luo et al. [40] reported for Pd/CeO_2 catalysts prepared by impregnation the shift of the peak maximum from 70 to 170 °C with Pd content decreasing from 5 to 0.25%. Gopinath et al. [41] reported the position of the peak at 130 and 182 °C for 1% Pd/CeO_2 catalyst prepared by impregnation using nitrate and chlorine precursor, respectively. For Pd (0.5%) deposited by impregnation on CeO_2 nanoparticles (6–9 nm) or nanorods TPR profiles contained reduction peaks at 245 and 195 °C, respectively [42]. The authors assign the peaks to very small PdO particles, strongly interacting with CeO_2 surface.

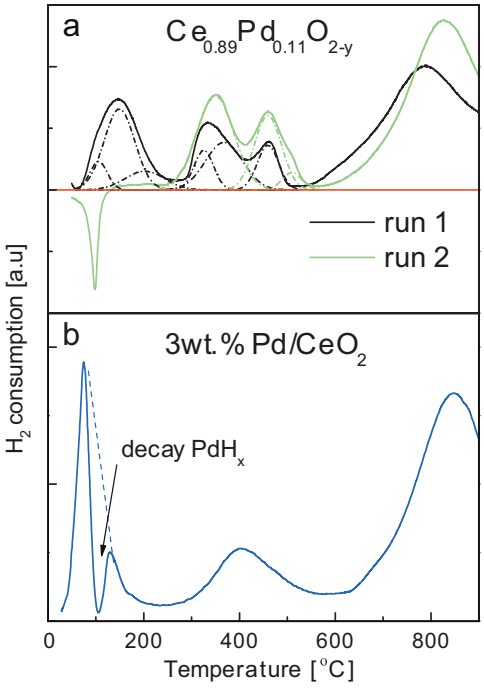

Fig. 13. H_2-TPR profiles of the "as-prepared" $Ce_{0.89}Pd_{0.11}O_{2-y}$ sample (a) and 3 wt% Pd/CeO_2 (b).

In the middle temperature region there is a two peaks: an overlap peak with two maxima at 325 and 367 °C and peak at 460 °C. This ceria surface reduction peaks are similar to that observed in TPR profiles of nanocrystalline CeO_2 doped with lanthanide ions [43] but is shifted toward lower temperature. These peaks are assigned to reduction of surface and subsurface layers of ceria. It appears that for 3 wt% Pd/CeO_2 in this temperature range there is much weaker broad single peak at ~410 °C. Finally, for $Ce_{0.89}Pd_{0.11}O_{2-y}$ there is also a broad, high temperature peak above 600 °C, with maximum at 780 °C. The peak is similar to that for 3 wt% Pd/CeO_2 but is shifted to lower temperatures. The peak is assigned to bulk reduction of ceria.

3.4.3. II H_2-TPR run for $Ce_{0.89}Pd_{0.11}O_{2-y}$ sample

Completion of the first TPR run (heating in reducing atmosphere up to 920 °C) followed by re-oxidation at 500 °C for 0.5 h caused significant change in the next TPR profile. The low temperature peak at 150 °C disappeared completely and a negative peak at 70 °C occurred instead. The negative peak is commonly assigned to decomposition of Pd hydride phase that is formed at lower temperatures. The process of hydride formation, as well as preceding reduction of PdO is not observed in our case due to limitations of the instrument, but it is clear, that it occurs at lower temperature than for 3 wt% Pd/CeO_2. It is consistent with the structure data showing that treatment in hydrogen at high temperature (≥800 °C) caused segregation of Pd from $Ce_{0.89}Pd_{0.11}O_{2-y}$ lattice and formation of large Pd particles (Table 2). Most probably Pd ions have been pulled out from surface or near surface region because there is no reduction peak responsible for reduction of surface Pd^{2+} ions in the TPR profile (peak at 150 °C in the I-TPR run). There was some increase of intensity of the medium temperature peaks and shift of the high temperature peak toward higher temperatures. Observed increase of the medium temperature peak could be accounted for with promoting effect of Pd particles on surface reduction of CeO_2 (hydrogen spill-over). Finally upward shift of the high temperature peak is caused by crystallite growth (sintering) of ceria during the first TPR run. The most important observation is that despite drastic treatment (TPR run up to 920 °C) the middle temperature reduction

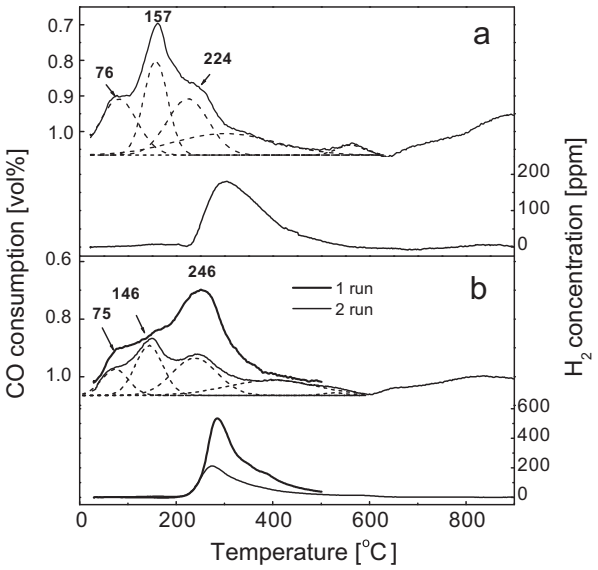

Fig. 14. CO-TPR profiles of 3% Pd/CeO_2 imp (a) and $Ce_{0.89}Pd_{0.11}O_{2-y}$ (b).

features increased in intensity pointing to stable, high OCS activity of Pd doped ceria.

3.4.4. CO-TPR

CO-TPR is one of the best probes to investigate the reducibility of Pd-ceria catalysts for CO-involved reactions and is helpful to identify the surface oxygen species and the finely dispersed surface PdO_x and Ce—Pd—O surface species [7,40,44] since the effect of spillover is weaker for CO than for hydrogen [45]. Generally, a consumption of CO during the CO-TPR process is accompanied with formation of CO_2 and H_2. H_2 and CO_2 may be produced in WGS reaction due to the interaction of CO adsorbed on Pd with the hydroxyl groups at the catalyst surface. WGS reaction is believed to take place at the metal–support interface [46].

$$CO_{(Pd)} + 2OH^- \rightarrow CO_{2(g)} + H_{2(g)} + O^{2-}$$

CO_2 may also form through either the reduction of reducible species such as PdO and ceria or the disproportionation of CO (Boudaurd reaction).

$$CO + PdO \rightarrow Pd + CO_2$$

$$\delta CO + CeO_2 \rightarrow CeO_{2-\delta} + \delta/2CO_2$$

$$2CO \rightarrow CO_2 + C$$

Fig. 14 shows CO-TPR traces from fully oxidized 3% Pd/CeO_2 (imp) (a) and $Ce_{0.89}Pd_{0.11}O_{2-y}$ (b) samples, where consumption of CO and production of hydrogen are plotted as function of temperature. For both samples CO consumption occurs in a whole temperature range, exhibiting nearly six peaks centered at ca. 80, 150, 250, 400, 550 °C and very broad feature at 600–900 °C.

For 3% Pd/CeO_2 sample (Fig. 14a) the first peak at 76 °C is related to reduction of PdO_x surface phase, and peaks at 157 and 224 °C are assigned to reduction of PdO_x species with various strength of interaction with the ceria support or different particle size. The later peak at 224 °C is also accompanied by evolution of hydrogen (see insets to Fig. 14) which is partly due to the WGS reaction. Further broad peaks at ca. 350 and 600 °C can be assigned to Pd-catalyzed, surface reduction of nanocrystalline ceria support. Finally, the broad feature at 600–920 °C corresponds to bulk reduction of ceria ($\delta CO + CeO_2 \rightarrow CeO_{2-\delta} + \delta/2CO_2$).

For $Ce_{0.89}Pd_{0.11}O_{2-y}$ sample two successive CO-TPR profiles were recorded (Fig. 14b). In the first run the peak at 75 °C is similar to that for 3% Pd/CeO_2 and is linked mainly to reduction of traces of PdO_x at the surface of the mixed oxide. Further palladium ions substituting for Ce ions in the ceria lattice form Pd—O—Ce connections which are more stable than Pd—O bonds in Pd oxide. It causes the shift of the CO consumption peak to higher temperature (246 °C). As for 3% Pd/CeO_2 (imp) this peak is correlated with hydrogen emission due to WGS reaction, but its intensity is much higher. Correspondingly, intensity of the H_2 emission is also higher (cf., different scales on H_2 concentration axis). This observation shows very high activity of the mixed oxide in WGS reaction. First run of CO-TPR on $Ce_{0.89}Pd_{0.11}O_{2-y}$ sample was finished at 500 °C and then after re-oxidation (at 500 °C) the second CO-TPR run was performed up to 920 °C. It is seen that the profile of CO consumption resembles that for 3% Pd/CeO_2 (imp) indicating that redistribution of Pd in the surface region occurred during the first CO-TPR run leading probably to segregation of Pd and formation of very small Pd particles at the surface. Interestingly, there was dramatic decrease of the CO consumption at ~250 °C, where WGS reaction occurred. The reason must be depletion of the OH groups at the surface after the first CO-TPR run. The broad peak observed at 400 °C with small shoulder at 550 °C, which can be assigned to Pd-catalyzed, partial surface reduction of nanocrystalline ceria support is more intense than for 3% Pd/CeO_2 (imp). The high-temperature, broad feature at the range 600–920 °C is very similar to that for 3% Pd/CeO_2 (imp), indicating that the presence of Pd does not affect markedly the extraction of oxygen from the bulk at high temperature. As mentioned above, one of the reactions involving CO consumption could be its disproportion (Boudard reaction), which brings about deposition of carbon. In Pd/CeO_2 system the carbon could be deposited at the surface of the catalyst (as deposits of various morphology and crystallinity) and/or within Pd lattice as PdC_x carbide [47,48]. It should be stated however, that maximum temperature achieved during CO-TPR (920 °C) exceeds the limit of PdC_x existence in CO atmosphere (620 °C [48]), so that the Pd carbide possibly formed could decompose.

In order to clarify the possibility of carbon deposition during CO-TPR experiment a TPO oxidation was performed (Fig. 15). The upper part of the figure shows the change in O_2 concentration during temperature ramp up to 900 °C, while the lower corresponding change in concentration of CO_2. Significant differences in behavior of $Ce_{0.89}Pd_{0.11}O_{2-y}$ and 3% Pd/CeO_2 are seen. TPO profile of the 3% Pd/CeO_2 shows large O_2 consumption peak at 80 °C, three weaker peaks at 252, 343 and 430 °C and a double O_2 evolution peak at 700 and 739 °C. The first, low temperature peak accounts for oxidation of Pd particles and probably also oxidation of CO adsorbed on Pd during cooling the sample after CO-TPR (in 1% CO/He). This statement is supported by the fact that total intensity of the high-temperature peaks (700 and 739 °C), arising from decomposition of PdO, is lower than that of the low temperature peak and by the presence of a corresponding peak in CO_2 concentration profile (see below). Origin of the middle temperature peaks between 200 and 500 °C is less obvious. TPO profiles of reduced Pd catalysts containing CeO_2 show maxima of O_2 consumption in the 200 and 500 °C range, which are assigned to reoxidation of some Pd interacting strongly with the support [49,50]. For Pd particles weakly interacting with the support oxidation occurs at much lower temperatures (below 100 °C) [49,50]. We believe that O_2 consumption at 200 and 500 °C is in our case due to oxidation of various carbon deposits formed during CO-TPR as the result of the Boudard reaction. Maxima of CO_2 evolution shown in Fig. 15 clearly support this supposition. In this context behavior of the $Ce_{0.89}Pd_{0.11}O_{2-y}$ sample is quite different. Both low temperature O_2 consumption and high temperature O_2 evolution peaks are significantly smaller and shifted toward higher temperatures. Considering the fact that

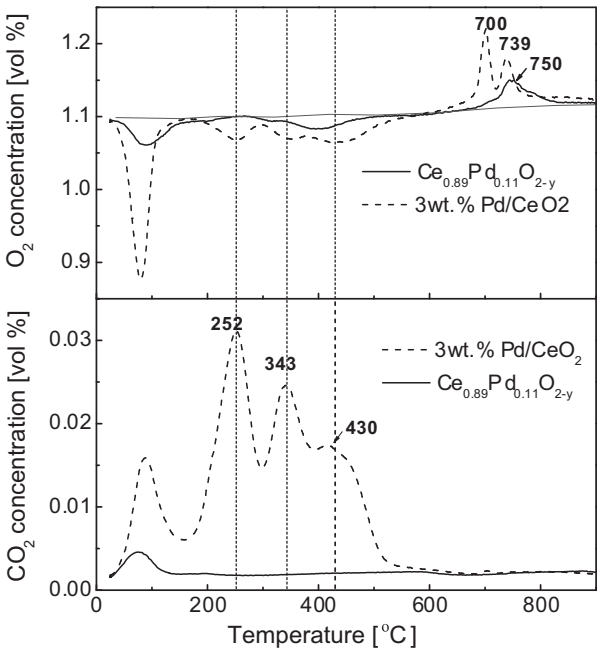

Fig. 15. TPO profiles (upper) and CO_2 concentration changes (lower) of 3% Pd/CeO_2 imp and $Ce_{0.89}Pd_{0.11}O_{2-y}$ samples.

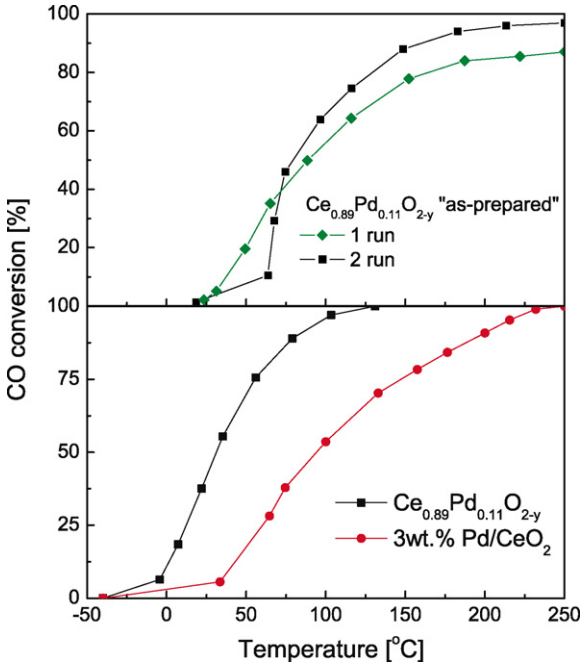

Fig. 16. CO conversion as function of temperature over "as prepared" $Ce_{0.89}Pd_{0.11}O_{2-y}$ 1st and 2nd run (upper part) and over $Ce_{0.89}Pd_{0.11}O_{2-y}$ and 3% Pd/CeO_2 (imp) reduced at 400 °C in H_2 (lower part).

the profiles of both samples are normalized to the same amount of Pd it means that only certain part (about half) of Pd is reduced in $Ce_{0.89}Pd_{0.11}O_{2-y}$ during CO-TPR. The shift of the peaks is probably related to stronger interaction of Pd with ceria. In middle temperature range there is a double peak of O_2 consumption at 313 and 404 °C. Interestingly, contrary to 3% Pd/CeO_2, this peak is not correlated with noticeable CO_2 production and cannot be ascribed to oxidation of carbon deposits, but rather to re-oxidation of ceria. This is important observation indicating that the $Ce_{0.89}Pd_{0.11}O_{2-y}$ mixed oxide may show high resistance to deactivation by carbon deposition. According to recent study [51] the enhanced resistance of the mixed oxide to carbon deposition may be connected with a blockade of formation of PdC_x carbide. Using in situ, dynamic structural and spectroscopic techniques, the authors of [51] showed that the process of carbidization of small Pd particles supported on $CeZrO_4$ in CO atmosphere is drastically suppressed with respect to similar Pd particles on alumina. The reason is the supply of oxygen from the $CeZrO_4$ support, which oxidizes atomic carbon generated at the surface of Pd. Small low-temperature peak in CO_2 concentration profile is, similarly as for 3% Pd/CeO_2, due to oxidation of CO adsorbed on the surface of Pd particles formed during CO-TPR.

3.5. CO combustion

Fig. 16 (upper part) presents temperature dependence of CO conversion to CO_2 in two successive runs on "as-prepared" $Ce_{0.89}Pd_{0.11}O_{2-y}$ sample. In the first run CO oxidation starts at room temperature and increases gradually reaching 85% conversion at ~250 °C. In the second run activity of the sample is lower at low temperatures (below 80 °C) but then increases steeply attaining 90% conversion already at 150 °C. The observed improvement of the activity in the second run was similar to the effect of pretreatment reported for various Pd/CeO_2 catalysts [3,5] and thus additional experiments were done to clear this point. Fig. 16 (lower part) shows CO conversion curves for $Ce_{0.89}Pd_{0.11}O_{2-y}$ and 3% Pd/CeO_2 pre-reduced at 400 °C in H_2. It is obvious that this procedure dramatically improved the activity of $Ce_{0.89}Pd_{0.11}O_{2-y}$ so that measurable CO conversion occurred even below room temperature. A complete 100% conversion was achieved at ~120 °C. Interestingly, the classic 3% Pd/CeO_2 catalyst prepared by impregnation and reduced at the same conditions was noticeably less active. It may be argued that the difference in activity between the mixed oxide and the impregnated catalysts arises mostly from various Pd content (7 and 3 wt%, respectively). It should be remembered, however, that in the former Pd is distributed uniformly within the bulk of ceria, whereas in the later it sits at the surface only. Assuming that for the $Ce_{0.89}Pd_{0.11}O_{2-y}$ ca., 1 nm thick selvage of the particles with 5 nm diameter may actively participate in the catalytic reaction we obtain roughly the same amount of Pd involved. It appears therefore that disparate microstructure must determine differences in the activity of both samples. Analysis of H_2-TPR profile of the 3% Pd/CeO_2 samples (Fig. 13 lower part) shows that up to 400 °C most of Pd is reduced and forms metallic particles. In accordance TEM revealed the presence of Pd particles with size of about 3 nm in this sample heated in H_2 at 400 °C for 1 h (Fig. 17a). For $Ce_{0.89}Pd_{0.11}O_{2-y}$ H_2-TPR profile also has a broad H_2 consumption maximum at ~150 °C probably connected with reduction of Pd ions at the surface, but it does not result in formation of well defined three dimensional Pd particles. As expected XRD revealed no sign of any crystalline Pd phase in the $Ce_{0.89}Pd_{0.11}O_{2-y}$ reduced in H_2 at 400 °C (Table 2). HRTEM also did not show the presence of Pd particles of the type seen after reduction at 500 °C (cf., Fig. 9). However, some crystallites in $Ce_{0.89}Pd_{0.11}O_{2-y}$ reduced at 400 °C (Fig. 17b) show contrast features (distortions in lattice fringes of the ceria crystallites) that, according to image simulations performed by Bernal et al. [52], could be interpreted as very small metal particles. These results show that the presence of some at least partially reduced Pd species, or extremely small particles (<1 nm) at the surface of ceria is a necessary condition for low temperature activity in CO oxidation. Such Pd particles, possibly with flat quasi 2D morphology, would be are strongly bonded to the surface, e.g., exhibiting a special epitaxial orientation observed at higher temperatures (Fig. 9). Anyway, the nature of the active Pd species must be very special because prereduction at too mild conditions (such as those experienced during first run of CO oxidation up to 300 °C) does not improve much the activity.

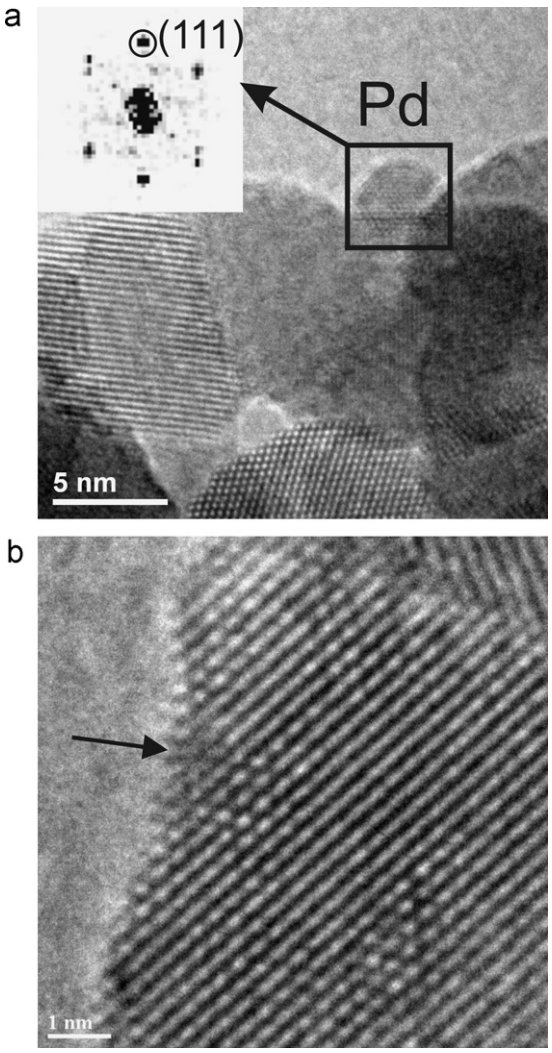

Fig. 17. HRTEM image of 3% Pd/CeO_2 (imp) (a) and $Ce_{0.89}Pd_{0.11}O_{2-y}$ (b) reduced at 400 °C in H_2. FFT pattern of a 3 nm Pd particle is shown as inset in (a).

Boronin et al. [3] showed that preliminary reduction of Pd/CeO_2 catalysts at 450 °C in hydrogen increased the activity in CO oxidation and assigned it to generation of very small (~1 nm), flat Pd islands strongly interacting with CeO_2. In line with our HRTEM data the metal islands show preferential orientation relative to ceria support [3]. According to [3] pre-reduction in H_2 may also generate specific hydroxyl groups located at the metal–support boundary, active in CO oxidation. Interestingly, Hinokuma et al. [5] observed that heating of Pd/CeO_2 catalyst in air at 900 °C also improved its activity in CO oxidation at low temperatures. The authors attributed this to special surface structures that form during such treatment. As the first step a Pd—O—Ce surface moiety appears due to interaction between PdO and CeO_2, which above 850 °C is fragmented into metallic 1–2 nm metallic Pd particles. Those particles are believed to provide active sites for CO oxidation [5]. The authors found also that direct reduction of the "as prepared" PdO/CeO_2 catalyst in hydrogen under mild conditions (below 400 °C) improved the activity [5]. The possibility of high temperature activation in oxidizing atmosphere seems to exclude principal role of hydroxyl groups in low temperature CO oxidation. Very recently, Meng et al. reported that minute PdO species existing at the surface of $Ce_{0.974}Pd_{0.026}O_{2-y}$ mixed oxide prepared by solution-combustion method are responsible for high activity in low temperature CO oxidation [53]. Removal of this surface species by dissolution in nitric acid decreased the activity in CO oxidation (shift of the CO conversion curve by ~50 °C to higher temperatures) indicating, in accordance with our data, that Pd^{n+} in Ce—Pd—O solid solution exhibits moderate activity in CO oxidation – similar to that of PdO/CeO_2 prepared by impregnation [53]. Literature data presented above clearly show that the nature of the surface sites active in low temperature CO oxidation (metallic or oxidized Pd) is still a matter of debate. The problem is complicated by the fact that catalyst activation may take place "in situ" during the catalytic reaction. For example DRIFT spectra of CO adsorbed on $PdO/Ce_{0.974}Pd_{0.026}O_{2-y}$ strongly suggest that CO may reduce the surface PdO species even at ambient conditions [53].

As the conclusion it seems that low temperature catalytic oxidation of CO on Pd-catalysts shows extreme sensitivity to the pretreatment history of the catalyst. In our case of the mixed $Ce_{0.89}Pd_{0.11}O_{2-y}$ oxide mild surface reduction which occurs during heating in H_2 at 400 °C provides metallic Pd sites necessary for CO adsorption and activation. On the other hand doping with aliovalent Pd ions and additionally reduction in hydrogen provide oxygen vacancies in ceria lattice responsible for O_2 activation [54]. Active role of oxygen vacancies in low temperature CO oxidation by nanocrystalline CeO_2 and Au/CeO_2 has been shown in recent "in situ" Raman study [55]. It may be concluded that a synergy of both kinds of active sites (small Pd metal islands and oxygen vacancies) explain high activity of the $Ce_{0.89}Pd_{0.11}O_{2-y}$ system in CO oxidation at low temperatures. Next step in elucidation of the detail mechanism of the reaction, including identification of reaction intermediates, would require microkinetics studies under precisely controlled reaction conditions [56].

4. Summary

We have shown, that using microemulsion method it is possible to prepare nanocrystalline $Ce_{1-x}Pd_xO_{2-y}$ mixed oxide with Pd content up to $x = 0.2$. XRD and HRTEM revealed that as prepared samples (subjected to annealing in oxygen at 500 °C) contain well developed crystallites with narrow size distribution and mean crystallite size 4–8 nm, decreasing with Pd content. The oxide with $x = 0.11$ showed no evidence of phase decomposition after annealing in oxygen at 800 °C and sintering strongly reduced in comparison with pure CeO_2. In hydrogen already at 500 °C, segregation of Pd at the surface was observed, with formation of small ~2 nm Pd particles preferentially oriented relative to ceria support. The epitaxial Pd (1 1 1)‖CeO_2 (1 1 1) orientation has been preserved even after reduction at 800 °C for Pd crystallites with size up to 8 nm. An important property of the $Ce_{0.89}Pd_{0.11}O_{2-y}$ is reversible extraction–dissolution of Pd upon successive reduction–oxidation cycles at 500 °C. This effect discovered for Pd-doped perovskite catalyst for automotive emission control [33] is a basis of so called "self-regenerative property" of vital importance for increasing a life-time of ceria based catalysts.

Nanocrystalline $Ce_{0.89}Pd_{0.11}O_{2-y}$ exhibits enhanced reducibility at low temperatures (below 500 °C), as compared to pure CeO_2. An important feature of $Ce_{0.89}Pd_{0.11}O_{2-y}$ is that this enhanced reducibility is preserved to large extent after treatment in hydrogen up to 930 °C, despite significant sintering of the oxide.

As prepared nanocrystalline $Ce_{0.89}Pd_{0.11}O_{2-y}$ demonstrates moderate activity in CO oxidation (starts at RT and increases gradually reaching 85% conversion at ~250 °C) similar to that of 3% Pd/CeO_2 prepared by impregnation. Activity of the $Ce_{0.89}Pd_{0.11}O_{2-y}$ in low temperature CO oxidation improves dramatically (measurable CO conversion below room temperature and 100% conversion at ~120 °C) after pre-reduction at 400 °C in H_2. It is believed that partially reduced Pd species, or extremely small particles (<1 nm) at the surface of ceria (not visible in XRD and TEM) are responsible

for the low temperature activity in CO oxidation. Such Pd species (particles) could be strongly bonded to the surface, e.g., exhibiting a special epitaxial orientation observed for larger Pd crystallites formed at higher temperatures. It appears that CO oxidation is very sensitive to the metal state and large variation in activity occurs depending on the catalyst pretreatment procedure. By using proper red-ox pretreatment the Pd may either be separated into Pd^0 metal nanoclusters, surface PdO species, or Pd^{2+}-like species incorporated in the CeO_2 lattice with oxide ion vacancy around Pd^{2+} ion. Such Pd^{2+} ion is highly stabilized in the Ce^{4+} site in the nanocrystalline $Ce_{1-x}Pd_xO_{2-y}$ solid solution forming —□—Pt^{2+}—O—Ce^{4+}— kinds of linkage. However, the exact nature of the active site is still under discussion which is closely related with fact that the synthesized catalysts usually contains a mixture of different Pd species. Experimentally observed high structural and chemical stability of nanocrystalline $Ce_{1-x}Pd_xO_{2-y}$ solid solution prepared as homogeneous mixed oxide makes it a promising catalyst of other important reactions occurring in fluctuating oxidation – reducing conditions.

Acknowledgments

The authors thank Mr. M. Ptak for recording Raman spectra and Dr. A. Gągor and Mrs. E. Bukowska for help with XRD work.

Appendix A. Supplementary data

Supplementary data associated with this article can be found, in the online version, at doi:10.1016/j.apcatb.2011.12.034.

References

[1] W. Shen, Y. Matsumura, Phys. Chem. Chem. Phys. 2 (2000) 1519–1522.
[2] W. Shen, Y. Ichihashi, M. Okumura, Y. Matsumura, Catal. Lett. 64 (2000) 23–25.
[3] A.I. Boronin, E.M. Slavinskaya, I.G. Danilova, R.V. Gulyaev, Y.I. Amosov, P.A. Kuznetsov, I.A. Polukhina, S.V. Koscheev, V.I. Zaikovskii, A.S. Noskov, Catal. Today 144 (2009) 201–211.
[4] S. Colussi, A. Gayen, M.F. Camellone, M. Boaro, J. Llorca, S. Fabris, A. Trovarelli, Angew. Chem. Int. Ed. 48 (2009) 8481–8484.
[5] S. Hinokuma, H. Fujii, M. Okamoto, K. Ikeue, M. Machida, Chem. Mater. 22 (2010) 6183–6190.
[6] S.-H. Oh, G.B. Hoflund, J. Catal. 245 (2007) 35–44.
[7] B. Wang, D. Weng, X. Wu, J. Fan, Catal. Today 153 (2010) 111–117.
[8] K.R. Priolkar, P. Bera, P.R. Sarode, M.S. Hedge, S. Emura, R. Kumashiro, N.P. Lalla, Chem. Mater. 14 (2002) 2120–2128.
[9] S. Roy, A. Marimuthu, M.S. Hedge, G. Madras, Appl. Catal. B: Environ. 71 (2007) 23–31.
[10] P. Singh, M.S. Hegde, Cryst. Growth Des. 10 (2010) 2995–3004.
[11] M.A. Małecka, L. Kępiński, W. Mišta, J. Alloys Compd. 451 (2008) 567–570.
[12] W. Rasband, ImageJ, U.S. National Institutes of Health, Bethesda, MD, USA, 1997–2007. Available from: http://rsb.info.nih.gov/ij/.
[13] R.D. Shannon, Acta Crystallogr. A 32 (1976) 751–767.
[14] J. Xu, J. Harmer, G. Li, T. Chapman, P. Collier, S. Longworth, S.C. Tsang, Chem. Commun. 46 (2010) 1887–1889.
[15] S. Deshpande, S. Patil, S.V.N.T. Kuchibhatla, S. Seal, Appl. Phys. Lett. 87 (2005) 133113.
[16] F. Zhang, S.-W. Chan, J.E. Spanier, E. Apak, Q. Jin, R.D. Robinson, I.P. Herman, Appl. Phys. Lett. 80 (2002) 127–129.
[17] J.E. Spanier, R.D. Robinson, F. Zhang, S.-W. Chan, I.P. Herman, Phys. Rev. B 64 (2001) 245407.
[18] J. Guzman, S. Carrettin, A. Corma, J. Am. Chem. Soc. 127 (2005) 3286–3287.
[19] J.R. McBride, K.C. Hass, B.D. Poindexter, W.H. Weber, J. Appl. Phys. 76 (1994) 2435–2441.
[20] A. Nakajima, A. Yoshihara, M. Ishigame, Phys. Rev. B 50 (1994) 13297–13307.
[21] M.A. Małecka, L. Kępiński, M. Mączka, J. Solid State Chem. 181 (2008) 2306–2312.
[22] J.R. McBride, K.C. Hass, W.H. Weber, Phys. Rev. B 44 (1991) 5016–5028.
[23] L. Barrio, A. Kubacka, G. Zhou, M. Estrella, A. Martinez-Arias, J.C. Hanson, M. Fernandez-Garcia, J.A. Rodriguez, J. Phys. Chem. C 114 (2010) 12689–12697.
[24] X. Wang, J.A. Rodriguez, J.C. Hanson, D. Gamarra, A. Martinez-Arias, M. Fernandez-Garcia, J. Phys. Chem. B 109 (2005) 19595–19603.
[25] W.H. Weber, K.C. Hass, J.R. McBride, Phys. Rev. B 48 (1993) 178–185.
[26] D.O. Scanlon, B.J. Morgan, G.W. Watson, Phys. Chem. Chem. Phys. 13 (2011) 4279–4284.
[27] J.A. Rodriguez, X. Wang, J.C. Hanson, G. Liu, A. Iglesias-Juez, M. Fernandez-Garcia, J. Chem. Phys. 119 (2003) 5659.
[28] M.A. Małecka, U. Burkhardt, D. Kaczorowski, M.P. Schmidt, D. Goran, L. Kępiński, J. Nanopart. Res. 11 (2009) 2113–2124.
[29] H. Zhang, J. Gromek, G.W. Fernando, H.L. Marcus, S. Boorse, J. Phase Equilib. 23 (2002) 246–248.
[30] R.J. Farrauto, M.C. Hobson, T. Kennelly, E.M. Waterman, Appl. Catal. A: Gen. 81 (1992) 227–237.
[31] S. Colussi, A. Trovarelli, E. Vesselli, A. Baraldi, G. Comelli, G. Groppi, J. Llorca, Appl. Catal. A: Gen. 390 (2010) 1–10.
[32] L. Kepinski, M. Wołcyrz, Appl. Catal. A 150 (1997) 197–220.
[33] T. Akita, M. Okumura, K. Tanaka, M. Kohyama, M. Haruta, Catal. Today 117 (2006) 62–68.
[34] R. Wang, P.A. Crozier, R. Sharma, J. Phys. Chem. C 113 (2009) 5700–5704.
[35] J. Ciston, R. Si, J.A. Rodriguez, J.C. Hanson, A. Martinez-Arias, M. Fernandez-Garcia, Y. Zhu, J. Phys. Chem. C 115 (2011) 13851–13859.
[36] Y. Nishihata, J. Mizuki, T. Akao, H. Tanaka, M. Uenishi, M. Kimura, T. Okamoto, N. Hamada, Nature 418 (2002) 164.
[37] M. Hatanaka, N. Takahashi, N. Takahashi, T. Tanabe, Y. Nagai, A. Suda, H. Shinjoh, J. Catal. 266 (2009) 182–190.
[38] G. Agostini, E. Groppo, A. Piovano, R. Pellegrini, G. Leofanti, C. Lamberti, Langmuir 26 (2010) 11204–11211.
[39] F. Pinna, F. Menegazzo, M. Signoretto, P. Canton, G. Fagherazzi, N. Pernicone, Appl. Catal. A 219 (2001) 195–200.
[40] M.-F. Luo, Z.-Y. Hou, X.-X. Yuan, X.-M. Zheng, Catal. Lett. 50 (1998) 205–209.
[41] R. Gopinath, N. Lingaiah, B. Sreedhar, I. Suryanarayana, P.S. Sai Prasad, Akira Obuchi, Appl. Catal. B: Environ. 46 (2003) 587–594.
[42] J.Y. Luo, M. Meng, H. Xian, Y.-B. Tu, X.-G. Li, T. Ding, Catal. Lett. 133 (2009) 328–333.
[43] M.A. Malecka, L. Kępiński, W. Mišta, Appl. Catal. B: Environ. 74 (2007) 290–298.
[44] M.-F. Luo, Z.-Y. Pu, M. He, J. Jin, L.-Y. Jin, J. Mol. Catal. A 260 (2006) 152–156.
[45] M.-F. Luo, X.-M. Zheng, Appl. Catal. A 189 (1999) 15–21.
[46] M. Cargnello, T. Montini, S. Polizzi, N.L. Wieder, R.J. Gorte, M. Graziani, P. Fornasiero, Dalton Trans. 39 (2010) 2122–2127.
[47] L. Kepinski, Catal. Today 50 (1999) 237–245.
[48] M. Maciejewski, A. Baiker, Pure Appl. Chem. 67 (1995) 1879–1884.
[49] M. Haneda, T. Mizushima, N. Kakuta, J. Phys. Chem. B 102 (1998) 6579–6587.
[50] R. Zhou, B. Zhao, B. Yue, Appl. Surf. Sci. 254 (2008) 4701–4707.
[51] M.A. Newton, M. Di Michiel, A. Kubacka, A. Iglesias-Juez, M. Fernandez-Garcia, Angew. Chem. Int. Ed., doi:10.1002/anie.201105790, in press.
[52] S. Bernal, J.J. Calvino, M.A. Cauqui, J.A. Perez Omil, J.M. Pintado, J.M. Rodriguez-Izquierdo, Appl. Catal. B 16 (1998) 127–138.
[53] L. Meng, A.P. Jia, J.Q. Lu, L.F. Luo, W.X. Huang, M.F. Luo, J. Phys. Chem. C 115 (2011) 19789–19796.
[54] Z.Y. Pu, X.S. Liu, A.P. Jia, Y.L. Xie, J.Q. Lu, M.F. Luo, J. Phys. Chem. C 112 (2008) 15045–15051.
[55] Y. Lee, G. He, A.J. Akey, R. Si, M. Flytzani-Stephanopoulos, I.P. Herman, J. Am. Chem. Soc. 133 (2011) 12952–12955.
[56] T. Baidya, A. Gupta, P.A. Deshpandey, G. Madras, M.S. Hegde, J. Phys. Chem. C 113 (2009) 4059–4068.